In-situ and Land-Based Remote Sensing of River Inlets and Their Interaction with Coastal Waters

Eric Terrill, Ph.D.
Director, Coastal Observing Research and Development Center
Marine Physical Laboratory
Scripps Institution of Oceanography
(858) 822-3101, eterrill@ucsd.edu

Award Number: N00014-10-1-0548
Award Number: N00014-13-1-0181

LONG-TERM GOALS

Principal research goals are to characterize the physics which control the river flow across the inlet and the fate of the plume within the coastal ocean. A by-product of the observational program will be the development of sensing capabilities that may have Naval interest.

OBJECTIVES

An observational program applying a broad suite of in-situ and boat-based remote sensing tools to the New River inlet and its interaction with the ocean was implemented during the RIVET I experiment. Of particular interest was the flow of the river through and within the inlet; wave breaking within the inlet as a result of shoaling and wave-current interactions; and the fate, dilution, and transport of the river plume as it discharges into the ocean. The discharge and its subsequent transport was dependent on volume, velocity, momentum and temporal variability of the flow; geometric characteristics of the inlet, channels and receiving waters; extent of a tidal prism within the inlet and influence of tides in modulating the flow; the ocean wave climate and wave current interactions and location of breaking within the inlet; and density differences between the river flow and the synoptic conditions of the coastal ocean into which it discharges. The goal was to develop and implement an observational program to best capture this dynamic and complex environment.

APPROACH

As a result of ONR-sponsorship over the past decade, a significant amount of ocean sensing technologies have been developed or acquired by PI Terrill that was utilized for RIVET I. A multi-sensor approach to the science program had the dual benefit of contributing to the development of appropriate river sensing strategies for future Naval applications.

WORK COMPLETED

X-band

Twenty-nine consecutive days (April 25 – May 23, 2012) of X-Band radar data was compiled by the SIO mobile radar van deployed on a beach adjacent to the New River Inlet. Data from the radar shows

Report Documentation Page

Form Approved
OMB No. 0704-0188

1. REPORT DATE	2. REPORT TYPE	3. DATES COVERED
30 SEP 2013		**00-00-2013 to 00-00-2013**

4. TITLE AND SUBTITLE	5a. CONTRACT NUMBER
In-situ and Land-Based Remote Sensing of River Inlets and Their Interaction with Coastal Waters	5b. GRANT NUMBER
	5c. PROGRAM ELEMENT NUMBER
6. AUTHOR(S)	5d. PROJECT NUMBER
	5e. TASK NUMBER
	5f. WORK UNIT NUMBER
7. PERFORMING ORGANIZATION NAME(S) AND ADDRESS(ES) **University of California, San Diego,Scripps Institution of Oceanography,9500 Gilman Drive,La Jolla,CA,92093**	8. PERFORMING ORGANIZATION REPORT NUMBER
9. SPONSORING/MONITORING AGENCY NAME(S) AND ADDRESS(ES)	10. SPONSOR/MONITOR'S ACRONYM(S)
	11. SPONSOR/MONITOR'S REPORT NUMBER(S)

12. DISTRIBUTION/AVAILABILITY STATEMENT
Approved for public release; distribution unlimited

13. SUPPLEMENTARY NOTES

14. ABSTRACT

15. SUBJECT TERMS

16. SECURITY CLASSIFICATION OF:			17. LIMITATION OF ABSTRACT	18. NUMBER OF PAGES	19a. NAME OF RESPONSIBLE PERSON
a. REPORT	b. ABSTRACT	c. THIS PAGE			
unclassified	**unclassified**	**unclassified**	**Same as Report (SAR)**	**13**	

along coast gradients in the wave breaking that are qualitatively found to correlate with geomorphologic shoreline features as evidence by the outline of the shoals. Backscatter was recorded at the highest resolution possible by the WAMOS digitizer: 3m range resolution, and 1/12 degree angular resolution. 1024 range samples were taken each angle, giving a range of over 3km from the RadarVan. 14TB of data was amassed overall. The radar data allows us to analyze the river inlet under the influence of varying river flows, tides, ocean currents, impending waves, and bathymetry.

REMUS AUV Surveys

A REMUS AUV (one equipped with inertial navigation - funded by a 2007 DURIP) was utilized for surveying the receiving waters. The vehicle was primarily used for characterizing water velocity and mapping the plume and its dilution in the receiving waters, however additional survey objectives included bathymetric and bottom-type characterization (sonar altimeter and sidescan). Twenty-six REMUS surveys were performed from May 2, 2012 through May 21, 2012. The primary objectives of the surveys were to map the spatial and temporal evolution of the river discharge into the receiving waters and well as support the Falk/Guza dye releases with additional in-situ observations outside of the inlet. Additional survey objectives included observations within the inlet, and sidescan sonar imaging of the seafloor.

Minature Wave Buoys

A fleet of four lightweight buoys capable of being moored or used as a drifter has been developed (2008 DURIP) and were used during the study. An array of buoys were deployed within the inlet to determine wave transformations in regions of high wave-current interaction. Buoys were deployed to drift across the shoals during all phases of tidal fluctuations. Figure 1 shows the tracks of all buoy deployments throughout the experiment The focus was to measure the transformation of the wave field as it crossed the tidal shoals and interacted with the inlet currents. Buoys were allowed to both ride in on the flood as well as be pushed out by the ebb tide. The three-directional velocity measurements allowed for wave paramenter observations and drift current measurements.

Figure 1. Buoy tracks for all deployments throughout the RIVET I experiment.

Wind Measurement Buoys

Three Iridium-reporting meteorological buoys were used to measure gradients of the wind field at the mouth of the inlet. A 1 meter mast keeps the instrument from submersion and shadowing within wave troughs. Three metereological buoys (Figure 2) were deployed to measure wind speed and direction as well as longshore wind shear. The closest inshore buoy was moored just offshore of the shoals. Met Buoy 02 was 1km offshore and Met Buoy 03 was 3km off shore to measure the wind speed undisturbed by friction from the land and shoaling waves.

Figure 2. The location of all three metereological buoys deployed off of the New River Inlet.

RESULTS

X-band

Averaging X-Band radar images provides a good indicator of shoaling wave activity in the river mouth. Using the USACE bathymetry, we define an ebb tide shoal line where the water depth decreases below 2m (see Figure 3).

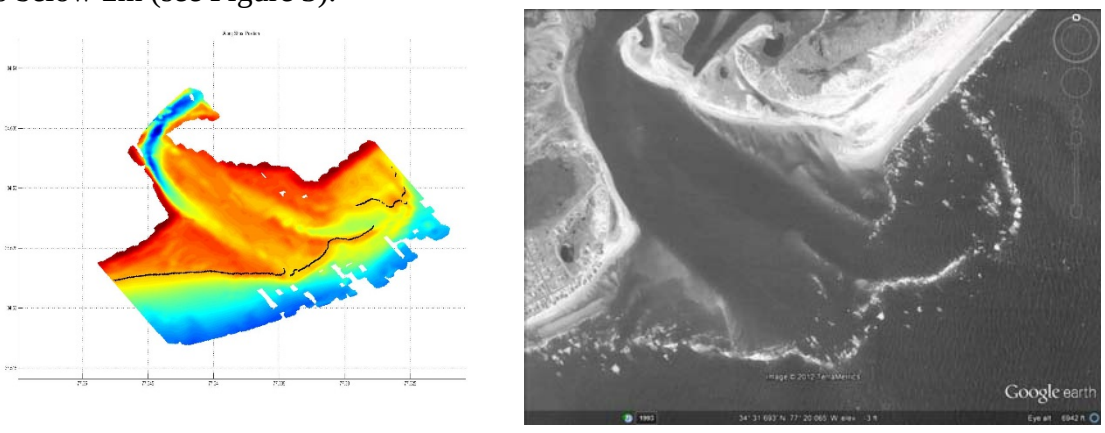

Figure 3. Left - Definition of the ebb tide shoal (black dots) Right – SAR Image showing white water shoaling area (courtesy Hans Graber, RSMAS)

By taking one minute averages and variances of the radar backscatter intensity along the ebb tide shoal definition over a 24 hour period, one can track the tides and water depth, and show where areas of potentially dangerous shoaling are occurring. Figure 4 shows the backscatter average data along the ebb tide shoal line, and the corresponding water depth from an in-situ pressure sensor deployed by WHOI.

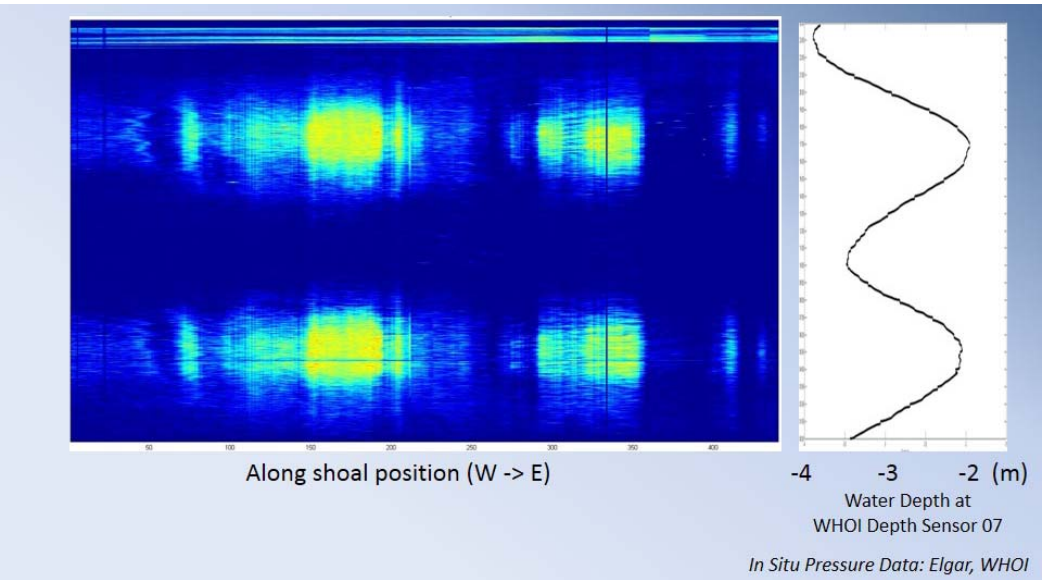

Figure 4. Backscatter average along ebb tide shoal line, showing varying shoaling activity, and observed water depth

Incident ocean wave analysis can be performed using the X-Band radar images. On May 19 at 16:30 UTC, the offshore CDIP buoy 190 was reporting the impending waves having a 1 meter significant wave height, 7.7s peak period, from 129 degrees. Using the X-Band backscatter from the New River channel marker buoy, and the SIO developed 3D wave inversion software, we can see the impending wave spectrum change as the ocean waves approach the river inlet. Figure 5 shows the wavenumber-frequency spectrum for that same time period.

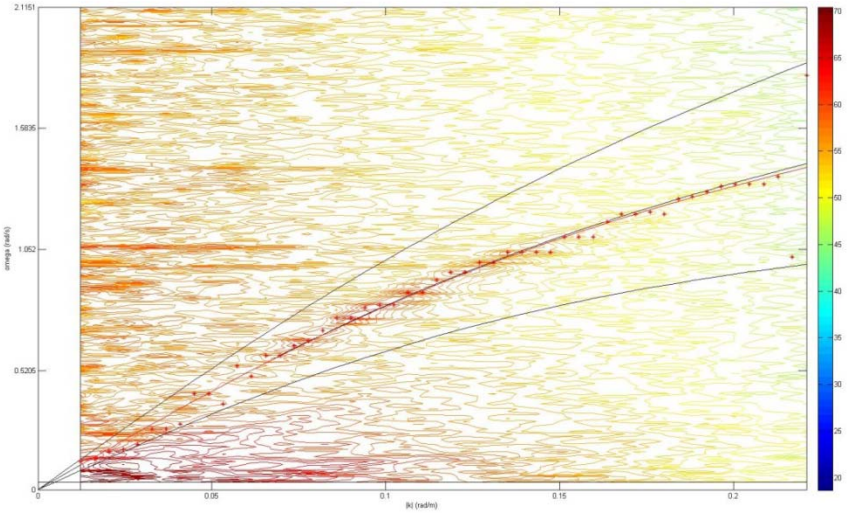

Figure 5. Wavenumber vs. frequency spectrum at the New River channel marker on May 19, 2012 at 16:30 UTC

In Figure 5, the red asterisks mark the peak of the spectral energy along a shifted dispersion relationship curve. In deep water, the waves reported by CDIP buoy 190 would have a wavenumber of 0.068 rad/m, a wavelength of 92m, and a celerity of 12 m/s. In this case the impending waves are shifted down in frequency by the outgoing tide and river plume, in addition the waves are shifted up in wavenumber due to the 8 meter water depth at the channel marker. The shifted dispersion relationship (middle black line) is then "flattened" out compared to the same waves in deep water.

Taking this analysis a step further, we can perform the same spectral analysis closer to shore over the shoals (Figure 6). Now the spectrum is even more linearized towards a very shallow dispersion relationship with tide and river plume (current) effects ($\omega=kh+\mathbf{k}\cdot\mathbf{U}$). An ongoing area of our research is to develop a non-linear inversion method to extract current and depth from these 3D X-Band image inversions. Preliminary efforts have shown some success, but the method still needs refining.

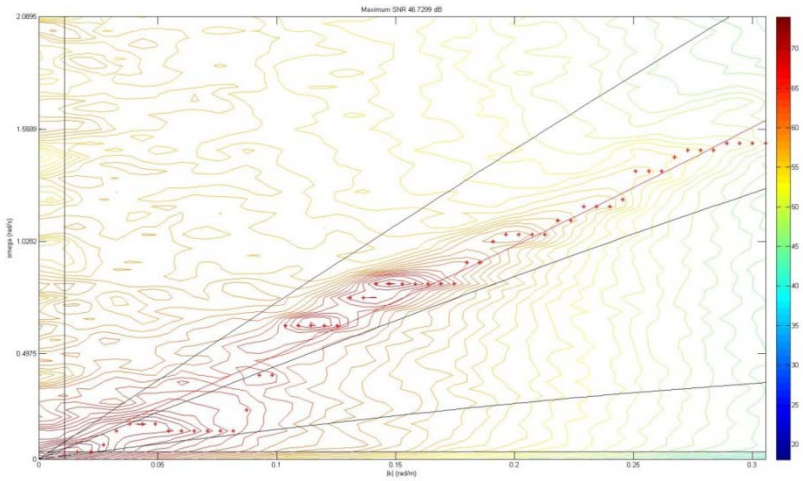

Figure 6. Wavenumber vs. frequency spectrum over the shoals at the mouth of the New River Inlet for May 19, 2012 at 16:30 UTC.

By completing the wave inversion, and plotting the resulting wave field over the shoal, we can produce Figure 7. This clearly shows the waves interacting with the shoals, as well as the old and new channels. The new channel has waves breaking across it at the ebb tide shoal line (previously defined).

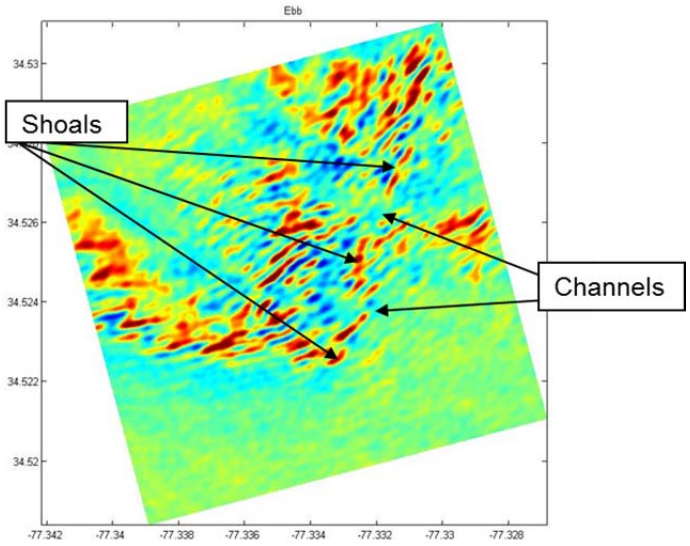

Figure 7. X-Band radar wave inversion results

In Figure 7, one cans see the impending waves shorten up in wavelength, progress throught the channels, refract towards (and break on) the shallow shoals. Previous research in current and bathymetry measurement using airborne imagery (Dugan, Pietrowski), X-Band radar (Bell), PIV analysis (Ahmed, Takewaka), and tomography (Plant, Holland, Haller) has proven effective in a linear shoreline environment. The complex bathymetry of the New River Inlet challenges those methods. Using concepts inherent in the literature, we can decompose the measured wavenumber frequency spectrum, and extract (filter) out a single frequency component, which has many wavenumber components contributing to it due to the bathymetry. By inverting this single frequency component back into the time domain, we can see how the bathymetry and current effect those singular waves. A simple ray tracing technique can be applied to the resulting images as shown in Figure 8.

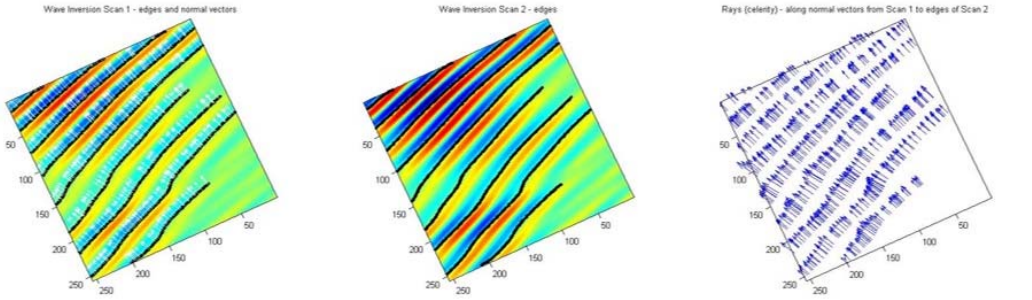

Figure 8. Ray tracing algorithm to determine wave celerity and bathymetry

The resulting celerity is then plotted in color over the USACE bathymetry in Figure 9. While not perfect, this simple method shows some promise to determine complex bathymetry with tidal and river current effects. Darker orange indicates higher celerity, yellow indicates lower celerity. One can see the waves slow down as they approach the shoal. Deeper channels and shallow mounds are also indicated in the celerity field. This is an ongoing area of our research.

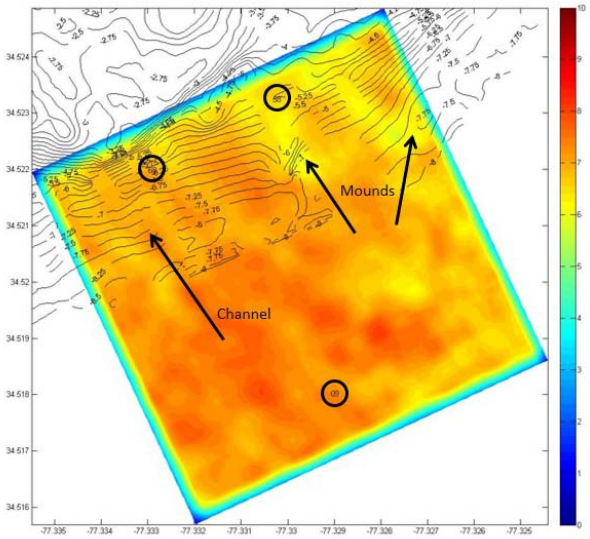

Figure 9. Celerity map and associated bathymetry

Moving on to determing seabed morphology, the radar backscatter intensity during low tide is being utilized to determine the movement of prominent features such as inlet navigation channels and shoaling regions. Figure 10 shows an example of a intensity image overlaid on bathymetry data from 5/2/2012. During low tide the images delineate the borders of the New River channels and shallow regions. Further analysis will focus on correlating the strength of the intensity observations with tidal stage and environmental conditions (e.g. wind speed and direction). Additional analysis will attempt to use X-band radar imagery to spatially map the movement of the shoals during the May 2012 experiment. Figure 11 shows a comparison between a 1-minute averaged radar image on 5/4/2012 and a 1-minute averaged image on 5/20/2012, both taken during similar environmental conditions (i.e. wind speed, direction, tidal stage). The figures suggest that the southern shoal (denoted by a red ellipse in Figure 11a) has lost sand near the boundary with the open ocean, but accumulated sand along the boundary with the inlet channel (denoted by red ellipse in Figure 11b). The depth increase due to the loss of sand will show up as a lower intensity signal while regions that become shallower can be tracked by higher intensity signals of the radar.

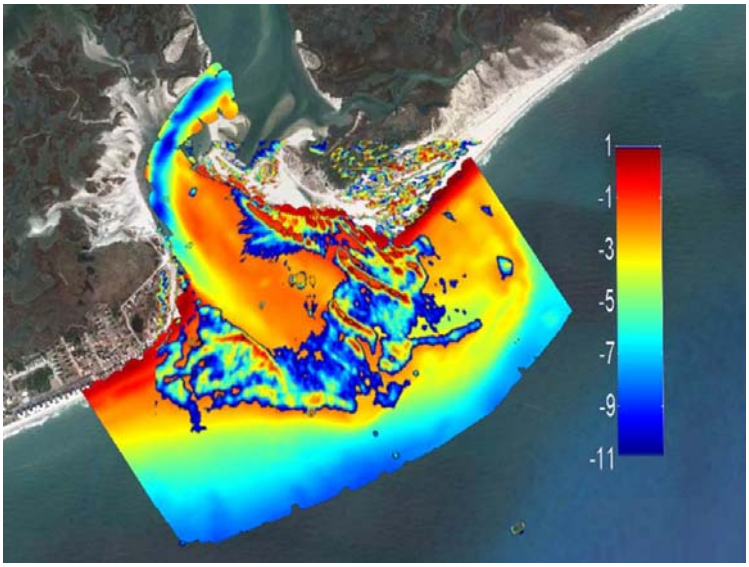

Figure 10. Overlay of X-band radar intensity imagery on bathymetry (in meters) observed by the US Army Corps of Engineers Field Research Facility on 5/2/2012. The radar intensity delineates the spatial boundaries of the inlet including shallow shoaling regions.

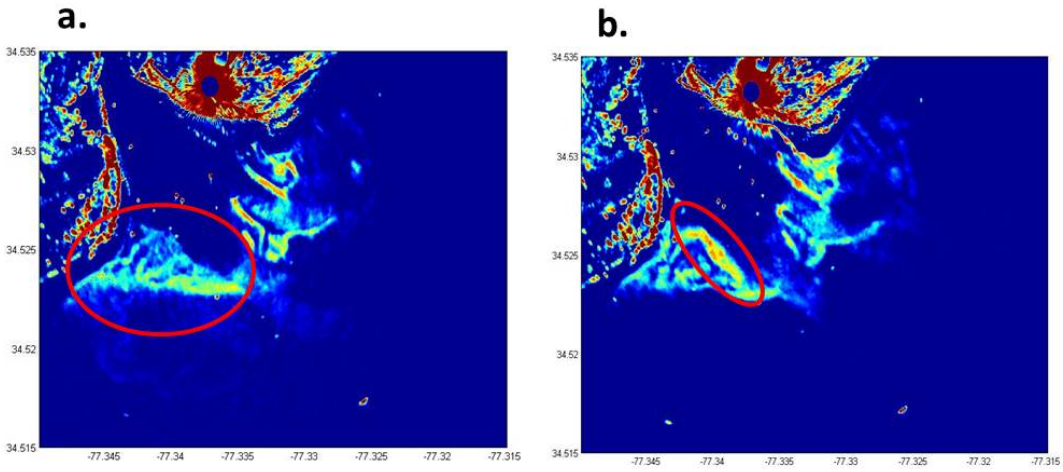

Figure 11. Comparison plot of 1-minute averaged radar imagery from (a) 5/4/2012 and (b) 5/20/2012 under similar environmental conditions.

REMUS AUV Surveys

The AUV was utilized to target the dynamic transitional region between the near and far-fields of the New River Inlet jet discharge during maximum ebb tide. A brief summary of results are presented below.

The composite Froude numbers of the near-field to far-field transitional region were computed from AUV observations for the 5/17/2012 and 5/19/2012 surveys and linearly interpolated between transects (Figure 12). The transition from the near-field to the far-field of a river plume is defined by the change of flow from supercritical to subcritical which is evident for both surveys. The 5/17/2012 survey (Figure 12a) was performed under ideal deployment conditions (i.e. minimal winds and waves) which yielded a clear transition from supercritical flow to subcritical that occurs between transect 2 ($Fr > 1$)

and transect 3 (Fr < 1). A minimal area of Froude numbers greater than 1 can be seen along transect 3 suggesting that this marks the offshore extent of the near-field plume. Transect 1 is ~ 150 m from the exit of the New River dredged channel into the open ocean (located at the origin of the figure) yielding an approximate cross-shore near-field length scale of 550 m for the 5/17/2012 survey.

The 5/19/2012 survey was performed under significantly different background conditions due to a sustained northeasterly wind of ~ 7 m/s resulting in challenging deployment conditions (high sea state). The observed Froude numbers from the survey suggest the wind acted to lengthen the near-field as seen by the supercritical flow in transect 4 (Figure 12b). The area of higher Froude numbers in transect 6 correspond with a more southwestward surface flow suggesting the localized wind stress is the dominant forcing mechanism confirming the transition into the far-field.

The effect of the differing wind conditions between each survey is also evident in the CDOM signature of the plume as it advects offshore. Figure 13 shows the progression of the plume from near-shore (transect 1, top figure) to offshore with an approximate spacing of 200 m and 240 m between each successive transect for the 5/17/2012 and 5/19/2012 surveys respectively. The CDOM signature in the core of the 5/17/2012 plume displays minimal variability with each successive transect until transect 6 (~ 1100 m from dredged channel) as illustrated in Figure 13a. Conversely, the 5/19/2012 CDOM plume signature undergoes significant mixing due to the momentum of the plume interacting with the ambient conditions caused by a strong northeasterly wind starting at transect 3 (~ 630 m from the dredged channel). The depth of each respective advecting plume suggests that stratification is also causing differences in the plume characteristics. In the far-field, the core of the 5/19/2012 plume is approximately two times the depth of the observed 5/17/2012 plume depth; ~2 m compared to ~4 m.

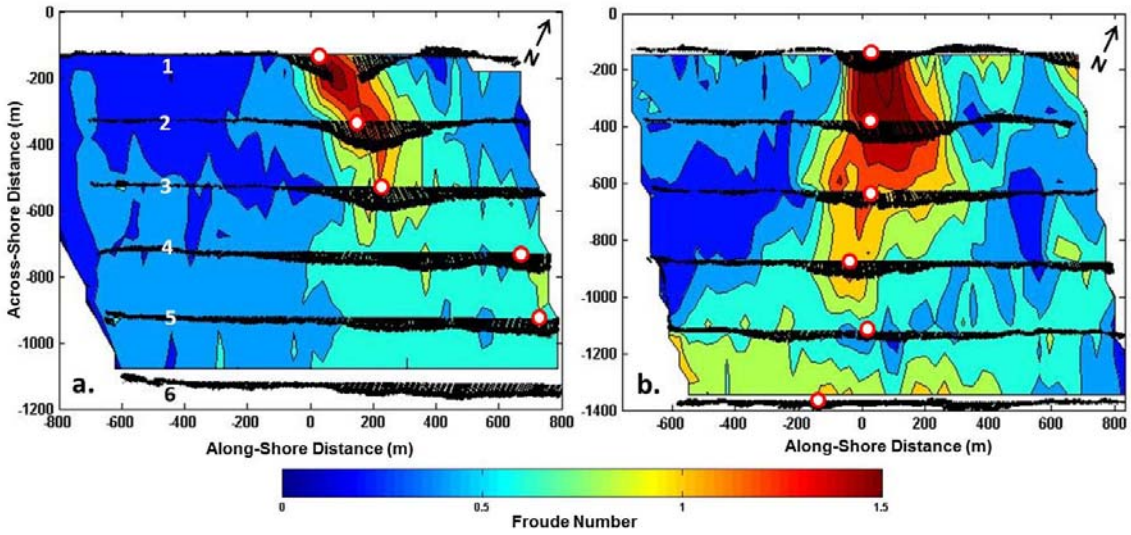

Figure 12. Linearly interpolated composite Froude number for the (a) 5/17/2012 and (b) 5/19/2012 surveys based on observed REMUS AUV velocity measurements (black arrows). Each transect in (a) is labeled with a transect number (1 thru 6). Red circles denote areas of interest for the Richardson number calculations discussed in Section 4.2. The discharge origin is located at (0,0).

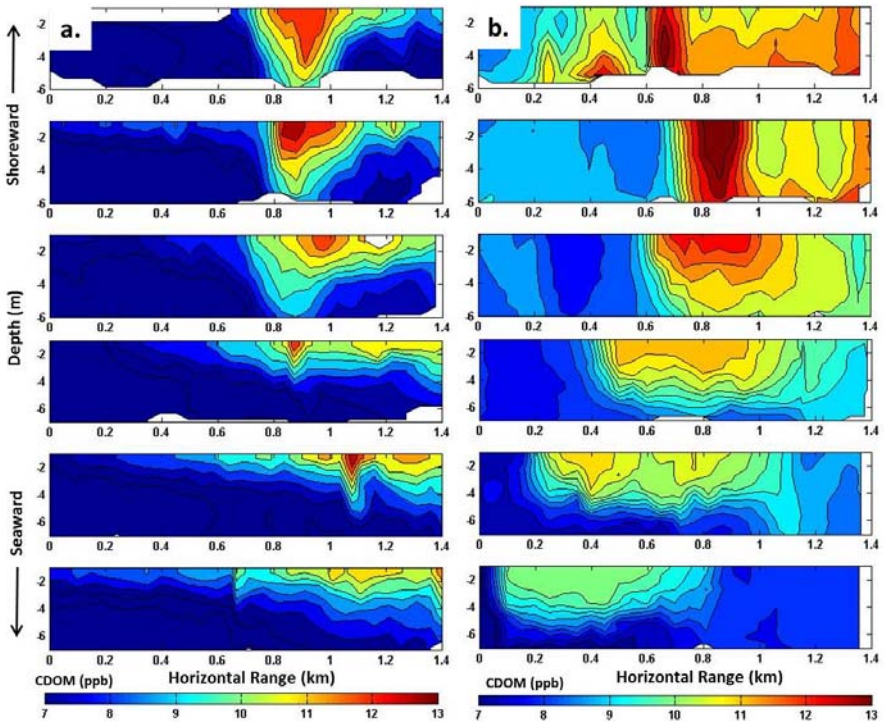

Figure 13. Observed CDOM contour plot of successive transects that followed the advecting plume offshore for the (a) 5/17/2012 and (b) 5/19/2012 surveys with transect spacing of ~200 m and ~240 m respectively.

The survey's results suggest that ambient ocean conditions (i.e. localized stratification, wind, and current) strongly influence the near-field and far-field characteristics of the discharged plume as it advects offshore. The mobility of the AUV coupled with modern observational instrumentation enabled detailed characterization and analysis of the plume and its mixing at a resolution not possible by conventional mapping techniques. The methods utilized to observe the dynamic variability of the transitional region can provide benchmark datasets for testing within coastal circulation models. Potential improvement of the method will come from future REMUS ADCP velocity experiments that will quantify the directional and velocity errors observed during vehicle undulation. The objective of the work will be to increase the accuracy of undulating survey velocity observations with the goal of eliminating repeat constant depth surveys yielding more synoptic datasets

Minature Wave Buoys

The wave parameters were studied using the wave buoy velocity measurements as the waves encountered the shoals and tidal currents. Figure 14 is an example of such observations, taken along a single buoy track shown in the right panel. The buoy track in red is overlayed on the satalite image as well as a 1-minute variance map of the X-Band backscatter at the time of buoy deployment. The X-Band variance is shown to visualize where the wave breaking is occuring. The top left panel shows directional spreading of the incoming waves as a function of frequency on the vertical axis and distance along buoy path on the horizontal. Also shown for this buoy path are significant wave height (middle panel) and ground speed (lower panel). The directional spreading shows the expected result that the wave direction becomes broader as waves are defracted by the bathymetry and currents.

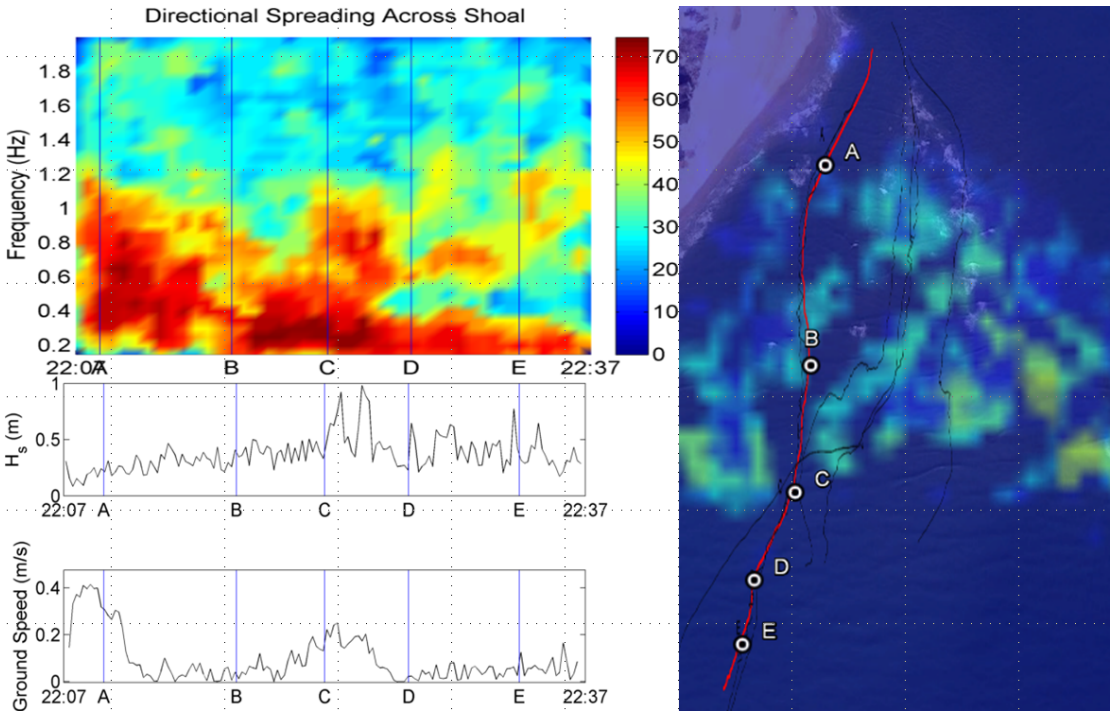

Figure 14. Directional spreading from buoy velocities as a buoy crosses the shoal on an ebb tide. The area of wave breaking is marked by the high X-Band variance in the underlaying checkerboard plot.

The observation of wave transformations across the shoals was also compared to the X-Band observations of the area. The return energy along the buoy path above was compared to the significant wave heights as seen by neighboring buoys at the same time. Figure 15 is the result, where the radar return is scaled for comparison. There is an obvious consistent peak on all observations, which corresponds to the edge of the shoal, where the incoming waves begin to feel the effects of the bathymetry and stand up.

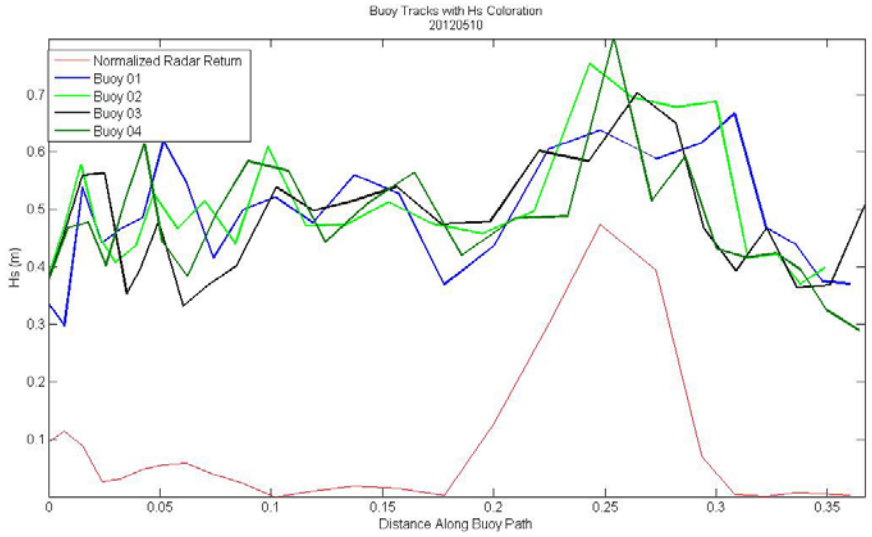

Figure 15. A comparison between X-Band return and miniature wave buoy significant wave height along a buoy path.

Wind Measurement Buoys

The 1m wind was measured throughout the experiment and can be used in conjunction with the wave buoy wave transformation measurements to support a model such as COAMPS for validation. Figure 16 shows the effect of the higher friction near shore as it compares the offshore and near shore buoy measurements. The structure of the wind fluctuations show that this is not a simple diurinal coastal system.

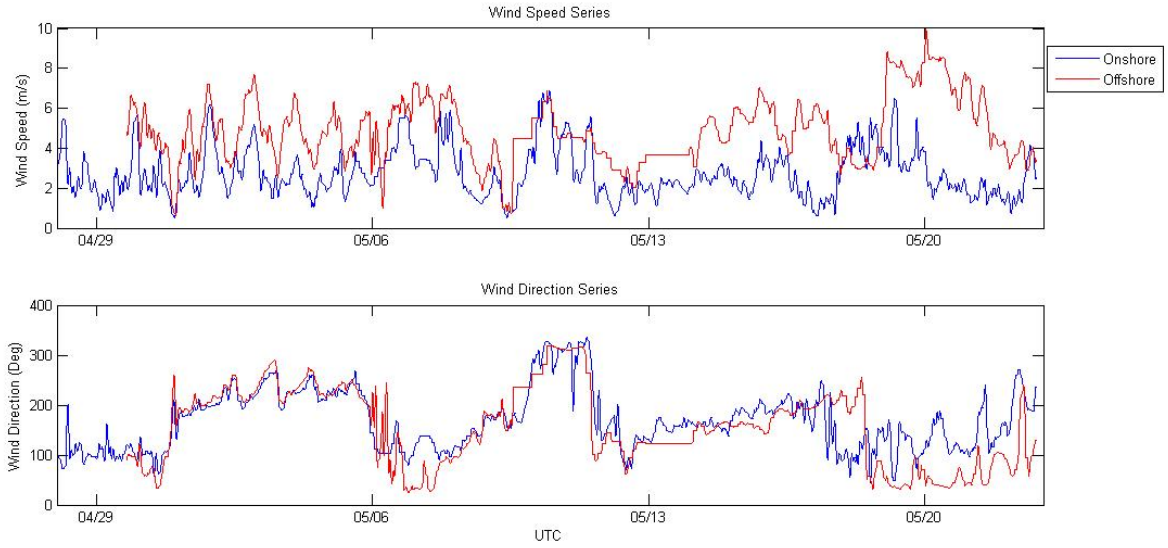

Figure 16. Offshore on near shore wind measurement comparisons

As the incoming wave field meets the river current offshore of the inlet, the waves become steeper and taller. This increases the coefficient of friction, slowing the wind as it approaches the shore. This effect is seen above after 5/20 when the wind direction is onshore. The large difference between buoys 1 and 3 is partially due to the slowing of the wind as it blows over the waves as the waves approach the inlet and become steeper.

IMPACT/APPLICATIONS

X-Band Radar

A data set of this size and resolution is a valuable asset for riverine science. We have the capability to track and measure relative water depth and shoaling activity through simple image averaging. This alone shows that X-Band radar can be used as a real time, remote sensing, river inlet hazard avoidance tool for mariners when visibility is limited. Additionaly, bottom morphology can be tracked by time series of backscatter averages over long periods of time. 3D spectral inversions can be used to remotely sense the change in impending waves, and therfore imply current and bathymetry measurements. Phase resolved wave inversions can accurately show wave refraction, breaking, and shoaling activity. Through a very narrow band frequency inversion, single wave trains can be analyzed through ray tracing for celerity to infer current and depth as well. Research is ongoing and methods are being improved and refined. We are looking forward to applying this research to the Mouth of the Columbia River.

REMUS AUV Surveys

AUV observations of the receiving waters of the New River Inlet yielded high resolution datasets of the dynamic mixing region where momemtum forces from the river discharge jet interact with the ambient ocean waters. There is potential to yield more synoptic datasets by improving velocity observations while the vehicle is undulating. Accurate velocity observations while the vehicle is sampling the water column would eliminate the need for repeat surveys at a constant depth, thus reducing mission time by approximately 50%.

Minature Wave Buoys

The ability of wave buoys to measure wave properties in the surf zone is a novel advancement and will has a potential for supplementing wave models. The current wave models lack validation for areas of shoaling wave transformation such as the above directional spreading and significant wave height.
The comparisons to X-Band backscatter are also an important new result in a shoaling environment. In both deep and shallow water, the mechanism for X-Band backscatter is similar and has been validated (HiRes project 2010). However, the good agreement between buoy significant wave height and X-Band return shows that X-Band radar can also be used to measure shoaling and breaking waves.

Wind Measurement Buoys

The effect of the steepening waves on the local coefficient of friction is a topic of continuing research. The observations made here are enough to suggest that an onshore wind will decelerate drastically as it encounters shoaling and steepening waves. The observation of the magnitude of this effect is a source of validation for a wind-wave coupled model.

RELATED PROJECTS

N00014-13-1-0198 In-situ and Land-Based Remote Sensing of River Inlets and Their Interaction with Coastal Waters: Mouth of Columbia River.

REFERENCES

Dugan, et. al., "Airborne Optical System for Remote Sensing of Ocean Waves", Journal of Atmospheric and Oceanographic Technology, Vol. 18, July 2001

Dugan, J.P., Piotrowski, C.C., Williams, J.Z., "Water depthe and surface current retrievals from airborne optical measurements of surface gravity wave dispersion", Journal of Geophysical Research, Vol. 106, No. C8, August 15, 2001

Piotrowski, C.C., Dugan, P.J., "Accuracy of Bathymetry and Current Retrievals From Airborne Optical Time-Series Imaging of Shoaling Waves", IEEE Transactions on Geoscience and Remote Sensing, Vol. 40, No. 12, December 2002

Dugan, J.P., Piotrowski, C.C, "Surface current measurements using airborne visible image time series", ELSEVIER Remote Sensing of the Environment, Vol. 84, 2003

Bell, P.S., "Shallow water bathymetry derived from an analysis of X-band marine radar images of waves", ELSEVIER Coastal Engineering, Vol. 37, 1999

Ahmed, A.S.M., Takewaka, S., "PIV Analysis of Filtered Radar Images to Derive Nearshore Wave Properties and Bathymetry at Hasaki, Japan", Coastal Dynamics, 2005

Plant, N.G., Holland, K.T., Haller, M.C., "Ocean Wavenumber Estimation from Wave-Resolving Time Series Imaging", IEEE Transactions on Geoscience and Remote Sensing, Vol. 46, No. 9, September 2008